

# MDL-GBG: A Non-parametric and Interpretable Granular-Ball Generation Method for Clustering

Zeqiang Xian, Caihui Liu\*, Yong Zhang, Wenjing Qiu, Duoqian Miao, and Witold Pedrycz *Life Fellow, IEEE*

**Abstract**—Existing granular-ball generation methods are still mainly driven by handcrafted quality measures and heuristic splitting or stopping criteria, which may weaken the transparency of local generation decisions in clustering. To address this issue, this paper proposes Minimum Description Length based Granular-Ball Generation (MDL-GBG), a non-parametric and interpretable granular-ball generation method for clustering. MDL-GBG reformulates granular-ball generation as a local model selection problem under the Minimum Description Length principle. For each granular ball, three candidate explanations are compared, namely a single-ball model, a two-ball model, and a core-ball-plus-residual model, and the model with the shortest description length is selected. In this way, ball retention, splitting, and residual peeling are unified within a common coding-theoretic framework. A residual reassignment mechanism is further introduced to re-evaluate peeled-off boundary samples after stable granular-balls are formed. Experiments on 20 UCI datasets show that the stable granular-balls generated by MDL-GBG provide an effective upstream representation for clustering. In particular, MDL-GBG+AC achieves the best average ranks in ARI, ACC, and NMI among the compared methods. These results indicate that MDL-GBG offers a principled and interpretable alternative to heuristic granular-ball generation strategies.

**Index Terms**—Granular-ball computing , minimum description length , local model competition , interpretable clustering , non-parametric algorithm

## I. INTRODUCTION

CLUSTERING is a fundamental task in unsupervised learning that aims to reveal the intrinsic organization of unlabeled data [1]. As real-world datasets continue to grow in scale, dimensionality, and structural complexity, however, traditional point-wise clustering methods face increasing challenges from two closely related issues [2], [3]. First, sample-level computation often incurs substantial time and memory costs. Second, noise, heterogeneous densities, weak inter-point connections, and non-convex structures can make local geometric relationships highly unstable. These challenges have motivated the exploration of representations beyond individual samples, so that local regions can be described in a more compact and structurally meaningful way.

Zeqiang Xian, Caihui Liu, Yong Zhang, and Wenjing Qiu are with the Department of Mathematics and Computer Science, Gannan Normal University, Ganzhou 341000, Jiangxi, China, and also with the Key Laboratory of Data Science and Artificial Intelligence of Jiangxi Education Institutes, Gannan Normal University, Ganzhou 341000, Jiangxi, China (e-mail: [xianzeqiang@gnnu.edu.cn](mailto:xianzeqiang@gnnu.edu.cn); [liucaihui@gnnu.edu.cn](mailto:liucaihui@gnnu.edu.cn); [zhang\\_yong@gnnu.edu.cn](mailto:zhang_yong@gnnu.edu.cn); [wenjingqiu@gnnu.edu.cn](mailto:wenjingqiu@gnnu.edu.cn)).

Duoqian Miao is with the Department of Computer Science and Technology, Tongji University, 201804 Shanghai, China (e-mail: [dqmiao@tongji.edu.cn](mailto:dqmiao@tongji.edu.cn)).

Witold Pedrycz is with the Department of Electrical and Computer Engineering, University of Alberta, Edmonton, AB T6R 2V4, Canada (e-mail: [wpedrycz@ualberta.ca](mailto:wpedrycz@ualberta.ca)).

\* Caihui Liu is the corresponding author.

Granular-ball computing provides a natural way to address these challenges. Instead of treating isolated samples as the basic computational units, it represents data by adaptive balls with different centers, radii, and coverage regions, thereby organizing local regions in a coarse-to-fine manner that is consistent with the global-first cognitive mechanism [4]. Early studies showed that using granular-balls rather than individual samples can reduce sample-level computation and improve robustness to local perturbations [5]. Subsequent work further established granular-ball computing as an adaptive multi-granularity representation and computation paradigm with advantages in efficiency, robustness, and interpretability [6], [7]. In this sense, granular-ball computing is not merely a compression-oriented approximation of the original data, but a structured local-region representation that provides a more stable and meaningful basis for downstream learning tasks.

This perspective has been widely adopted in clustering. Existing studies have incorporated granular-balls into spectral clustering, density peaks clustering, DBSCAN-style clustering, hierarchical clustering, manifold clustering, and multi-view clustering. In spectral clustering, granular-balls reduce the scale of graph construction and eigen-decomposition [8]. In density-based methods, they alleviate the cost of pairwise relation computation and improve scalability on large datasets [9], [10]. In structure-aware and multi-view settings, they also provide useful intermediate representations for capturing local topology and cross-view consistency [11], [12]. These studies suggest that granular-balls have gradually become an important intermediate structure that can directly influence clustering behavior and final performance.

As this line of research has developed, it has become increasingly clear that the effectiveness of granular-ball clustering is closely related to how granular-balls are generated. Granular-ball generation is therefore not merely a peripheral preprocessing step, but an upstream mechanism that affects whether local structures are represented faithfully and stably before clustering. Accordingly, substantial effort has been devoted to the design of generation strategies themselves.

Existing studies on granular-ball generation mainly follow two directions. One emphasizes efficiency and stability, for example through improved center selection or reduced dependence on repeated partition procedures [13], [14]. The other seeks better consistency between generated balls and the underlying data distribution, as exemplified by shortest-heterogeneous-distance-based generation, local-density-based generation, and granularity-tuning mechanisms [15]–[17]. More recently, the principle of justifiable granularity has been introduced into granular-ball generation, highlighting the balance

between coverage and specificity and inspiring regeneration-based and structure-aware extensions [11], [18], [19]. Collectively, these studies have enriched the methodological toolbox and improved empirical performance across a range of tasks.

Nevertheless, two methodological issues remain insufficiently addressed.

The first issue concerns parameter dependence and heuristic control. Although existing methods differ in form, many still rely on manually designed criteria such as purity, compactness, density, overlap, radius definition, neighborhood relations, or recursive stopping conditions [13]–[18]. While such criteria may capture certain aspects of local structure, they usually characterize only one structural facet at a time and therefore do not readily provide a unified principle for diverse local configurations. Moreover, even methods described as adaptive or parameter-free are often adaptive only within a predefined rule system, rather than being derived from a more general principle of structural explanation. As a result, when data simultaneously exhibit uneven densities, weak inter-point connectivity, mixed local patterns, or non-convex geometries, the behavior of existing methods may still depend heavily on empirical settings and often requires additional corrective mechanisms [11], [19], [20].

The second issue concerns interpretability at the generation-decision level. Granular-ball methods are often regarded as interpretable because the final balls have clear geometric meanings: their centers, radii, and coverage regions can usually be visualized directly [6]. However, result-level geometric intuition does not necessarily imply decision-level interpretability. In many existing methods, one may observe that a local region is ultimately represented by one ball or several balls, yet it often remains unclear why that particular decision is made. This issue is especially important in clustering, where a local region may correspond to substantially different structural situations: it may be genuinely single-centered, it may contain two local centers and therefore require splitting, or it may remain largely coherent while containing a few peripheral samples that should not dominate the local description. If these distinct situations are all judged by a single heuristic score, the generated granular balls may still appear geometrically intuitive, while the generation process itself remains insufficiently transparent.

This limitation is particularly relevant in clustering because, unlike classification, clustering lacks label information to regularize local representation decisions. As a result, each local decision in granular-ball generation may more directly influence the final clustering structure. If the generation rule is too conservative, heterogeneous local regions may be compressed into one ball, thereby obscuring latent substructures. If it is too aggressive, coherent local regions may be over-fragmented, reducing stability and introducing representational redundancy. If peripheral samples are indiscriminately absorbed into the main body, the radius and local dispersion of the ball may be unnecessarily inflated, which in turn can affect similarity estimation, graph construction, and ultimately cluster boundary formation. Recent developments in structure-aware clustering, natural-neighbor-assisted clustering, and regeneration-based granular-ball methods can be viewed as partial attempts to alleviate these difficulties [11], [19], [20]. Yet a more

general question remains open: how can one choose the most appropriate structural explanation for a current local region under a unified, non-empirical, and interpretable criterion?

To address this issue, this paper proposes a non-parametric and interpretable granular-ball generation method for clustering, termed Minimum-Description-Length-Based Granular-Ball Generation (MDL-GBG). The central idea is to reformulate granular-ball generation as a local model selection problem under the Minimum Description Length principle [21], [22]. Instead of deciding whether a current ball should be retained, split, or locally refined according to purity thresholds, density cutoffs, or overlap rules, MDL-GBG compares multiple candidate structural explanations and selects the one with the shortest description length. Specifically, each current granular-ball is evaluated under three candidate local models, namely a single-ball model, a two-ball model, and a core-ball-plus-residual model. In this way, local generation is governed not by a single handcrafted rule, but by explicit competition among structurally meaningful explanations.

This reformulation offers two potential advantages. First, it reduces dependence on empirical parameter settings, because retain, split, and residual-peeling decisions are all determined by a unified coding criterion rather than manually specified thresholds or task-specific constants. Second, it improves interpretability at the decision level, because each local regeneration step can be explained as the outcome of a coding trade-off among competing structural hypotheses. Accordingly, MDL-GBG is intended to make the generation process itself more interpretable, rather than relying solely on the geometric intuition of the final representation.

The main contributions of this work are summarized as follows.

- We propose MDL-GBG, a non-parametric granular-ball generation framework for clustering that reformulates granular-ball generation as a local model selection problem under the Minimum Description Length principle, thereby reducing reliance on purity thresholds, density parameters, and heuristic splitting rules.
- We construct three candidate local explanations, namely the single-ball model, the two-ball model, and the core-ball-plus-residual model, and unify retain, split, and residual-peeling decisions through a common description-length comparison mechanism.
- We enhance interpretability at the generation-decision level by making each local regeneration step explainable as a coding trade-off among competing structural hypotheses, rather than relying solely on result-level geometric intuition.
- We validate the proposed method in clustering scenarios and show that MDL-based local model competition can provide a more stable and structurally reasonable upstream granular-ball representation for complex unlabeled data.

The remainder of this paper is organized as follows. Section II presents the proposed MDL-GBG framework in detail, including the problem formulation, local modeling assumptions, the description-length formulations of the three candidate local explanations, the abnormal-ball criterion, and the overall algorithmic procedure. Section III analyzes the computational

complexity of the proposed method. Section IV describes the experimental settings and reports the clustering results on 20 UCI datasets. Section V provides discussion and concluding remarks, including the empirical characteristics, advantages, limitations, and future directions of MDL-GBG.

## II. METHODOLOGY

In this section, the proposed MDL-GBG framework is presented in detail. The core idea is to treat granular-ball generation as a local model selection problem under the Minimum Description Length principle. For each current granular-ball, several candidate structural explanations are evaluated under a unified coding criterion, so that retention, splitting, and residual peeling can all be determined within the same decision framework. The presentation starts from the problem formulation and basic assumptions, and then introduces the three local models, the abnormal-ball criterion, the regeneration strategy, and the overall procedure.

### A. Problem Formulation

Let  $X = \{x_1, x_2, \dots, x_n\}, x_i \in \mathbb{R}^d$  be the input dataset. The goal is to construct a stable granular-ball set  $\mathcal{G}^* = \{B_1, B_2, \dots, B_K\}$ , together with an optional residual set  $\mathcal{R}^* \subseteq X$ , such that each retained ball provides a concise and stable local representation of the data.

For the sample subset  $X_B$  covered by a current granular ball  $B$ , three candidate local explanations are considered:

- **Single-ball model**  $M_1$ : the local region is adequately represented by one compact ball;
- **Two-ball model**  $M_2$ : the local region contains two distinct local centers and is better represented by two sub-balls;
- **Core-ball-plus-residual model**  $M_3$ : the local region remains largely single-centered, but a small number of peripheral samples are better treated as residuals outside a core ball.

For each current granular ball  $B$ , the optimal local explanation is defined as

$$M^*(B) = \arg \min_{M \in \{M_1, M_2, M_3\}} L(M; X_B), \quad (1)$$

where  $L(M; X_B)$  denotes the description length of model  $M$  for encoding  $X_B$ .

### B. Normalization and Local Baseline Assumption

Because granular-ball centers, radii, shell volumes, and local variances are scale-dependent, each feature is first normalized by min–max scaling:

$$x'_{ij} = \frac{x_{ij} - \min(x_{.j})}{\max(x_{.j}) - \min(x_{.j})}, \quad j = 1, \dots, d. \quad (2)$$

On this basis, a normal granular ball is regarded as a locally single-centered structure without clear internal fragmentation, and is modeled by an isotropic Gaussian distribution:

$$x_i \stackrel{i.i.d.}{\sim} \mathcal{N}(c, \sigma^2 I_d), \quad (3)$$

where  $c \in \mathbb{R}^d$  denotes the ball center and  $\sigma^2$  is a common dispersion parameter. This assumption serves only as a parsimonious local baseline rather than a strict claim about the true data-generating distribution.

### C. Coarse-Grained Initialization

Before local MDL competition begins, a coarse initial ball set is constructed. This stage does not determine the final structure, but only provides initial regions for subsequent MDL-driven regeneration.

For any subset  $Y = \{y_1, \dots, y_m\} \subseteq \mathbb{R}^d$ , an approximate farthest-point bisection strategy is adopted. Let  $y^{(0)} \in Y$  be an initial point. The first farthest point is defined as

$$y^{(1)} = \arg \max_{y \in Y} \|y - y^{(0)}\|_2, \quad (4)$$

and the second farthest point is

$$y^{(2)} = \arg \max_{y \in Y} \|y - y^{(1)}\|_2. \quad (5)$$

The subset is then partitioned according to relative proximity to these two anchors:

$$Y_1 = \{y \in Y : \|y - y^{(1)}\|_2 \leq \|y - y^{(2)}\|_2\}, Y_2 = Y \setminus Y_1. \quad (6)$$

The above process is recursively applied until the number of initial balls reaches

$$k_0 = \max(1, \lfloor \sqrt{n} \rfloor). \quad (7)$$

This initialization is coarse by design and only serves to provide starting regions for subsequent local refinement.

### D. Adaptive Minimum Admissible Ball Size

To ensure sufficient sample support for local model comparison while avoiding a fixed empirical threshold, the minimum admissible ball size is adaptively defined as

$$n_{\min} = \max\left(2, \left\lceil \min\left(\frac{\sqrt{n}}{\ln(\sqrt{d+2})}, d+2\right) \right\rceil\right), \quad (8)$$

where  $n$  is the total number of samples and  $d$  is the feature dimension.

In Eq. (8),  $\sqrt{n}$  provides a basic sample-support scale, motivated by the common statistical fact that many fluctuations decrease at the rate  $1/\sqrt{n}$ . The term  $\ln(\sqrt{d+2})$  introduces a smooth correction for dimensional complexity, so that  $n_{\min}$  does not vary too aggressively in high-dimensional settings. Meanwhile,  $d+2$  has a direct parametric interpretation: the single-ball model requires estimating a  $d$ -dimensional center vector and one scalar variance, yielding  $d+1$  free parameters in total, and the extra  $+1$  provides a conservative margin for stable estimation.

### E. Basic Geometric Quantities

For any nonempty subset  $X_B = \{x_1, \dots, x_{n_B}\} \subseteq X$ , the center of granular ball  $B$  is defined as

$$c_B = \frac{1}{n_B} \sum_{i=1}^{n_B} x_i, \quad (9)$$

and its radius is defined as

$$r_B = \max_{1 \leq i \leq n_B} \|x_i - c_B\|_2. \quad (10)$$

### F. Single-Ball Model

For a sample subset  $Y = \{y_1, \dots, y_m\} \subseteq \mathbb{R}^d$ , the single-ball model assumes  $y_i \stackrel{i.i.d.}{\sim} \mathcal{N}(c, \sigma^2 I_d)$ . Its description length is defined as

$$L_1(Y) = -\log p(Y | \hat{c}, \hat{\sigma}^2) + \frac{k_1}{2} \log m. \quad (11)$$

This definition follows the Minimum Description Length principle, which balances data fidelity and model complexity. In Eq. (11), the first term is the coding cost of  $Y$  under the single-ball model, and a smaller value indicates stronger consistency with a compact single-centered structure. The second term is a BIC-style complexity penalty that reflects the cost of parameterization and avoids favoring a more flexible model solely because of likelihood improvement. Since the single-ball model contains a  $d$ -dimensional center and one scalar variance, its number of free parameters is  $k_1 = d + 1$ . Thus,  $L_1(Y)$  is the total description length of representing  $Y$  by a single compact granular-ball.

*Theorem 1:* Under the single-ball model, the maximum likelihood estimates are

$$\hat{c} = \bar{y} = \frac{1}{m} \sum_{i=1}^m y_i, \quad (12)$$

and

$$\hat{\sigma}^2 = \frac{1}{dm} \sum_{i=1}^m \|y_i - \bar{y}\|_2^2. \quad (13)$$

*Proof 1:* The joint density can be written as

$$p(Y | c, \sigma^2) = \prod_{i=1}^m \frac{1}{(2\pi\sigma^2)^{d/2}} \exp\left(-\frac{\|y_i - c\|_2^2}{2\sigma^2}\right). \quad (14)$$

Taking the negative logarithm yields

$$-\log p(Y | c, \sigma^2) = \frac{md}{2} \log(2\pi\sigma^2) + \frac{1}{2\sigma^2} \sum_{i=1}^m \|y_i - c\|_2^2. \quad (15)$$

Minimizing with respect to  $c$  is equivalent to minimizing  $\sum_{i=1}^m \|y_i - c\|_2^2$ , whose unique minimizer is the sample mean  $\bar{y}$ , which gives Eq. (12). Let

$$SSE(Y) = \sum_{i=1}^m \|y_i - \bar{y}\|_2^2. \quad (16)$$

Substituting  $c = \bar{y}$  into Eq. (15) gives

$$-\log p(Y | \bar{y}, \sigma^2) = \frac{md}{2} \log(2\pi\sigma^2) + \frac{SSE(Y)}{2\sigma^2}. \quad (17)$$

Differentiating with respect to  $\sigma^2$  and setting the derivative to zero yields

$$\hat{\sigma}^2 = \frac{SSE(Y)}{dm}, \quad (18)$$

which is Eq. (13).

Substituting the maximum likelihood estimates into Eq. (11) yields the closed form

$$L_1(Y) = \frac{md}{2} \left(1 + \log(2\pi\hat{\sigma}^2)\right) + \frac{d+1}{2} \log m. \quad (19)$$

### G. Two-Ball Model

When the current ball actually contains two local centers, the single-ball model tends to overestimate dispersion. In this case, a natural alternative is to partition the local region into two sub-balls.

Suppose that  $X_B$  is partitioned into two disjoint subsets  $Y_1$  and  $Y_2$ , satisfying  $Y_1 \cup Y_2 = X_B$ ,  $Y_1 \cap Y_2 = \emptyset$ . Let  $m_j = |Y_j|$ ,  $\pi_j = m_j/n_B$ ,  $j = 1, 2$ . The description length of the two-ball model is defined as

$$L_2(X_B; Y_1, Y_2) = L_{\text{part}}(Y_1, Y_2) + L_1(Y_1) + L_1(Y_2), \quad (20)$$

where the partition cost is

$$L_{\text{part}}(Y_1, Y_2) = n_B H(\pi_1, \pi_2), \quad (21)$$

with

$$H(\pi_1, \pi_2) = -\pi_1 \log \pi_1 - \pi_2 \log \pi_2. \quad (22)$$

*Theorem 2:* For a binary partition of size  $n_B$ , if the two parts contain  $m_1$  and  $m_2$  samples, respectively, then

$$\log \binom{n_B}{m_1} = n_B H(\pi_1, \pi_2) + o(n_B), \quad (23)$$

where  $\pi_j = m_j/n_B$ .

*Proof 2:* By Stirling's approximation,

$$\log n! = n \log n - n + o(n), \quad (24)$$

we have

$$\log \binom{n_B}{m_1} = \log n_B! - \log m_1! - \log m_2!. \quad (25)$$

Substituting Stirling's formula yields

$$\log \binom{n_B}{m_1} = n_B \log n_B - m_1 \log m_1 - m_2 \log m_2 + o(n_B). \quad (26)$$

Let  $m_j = n_B \pi_j$ . Then

$$\begin{aligned} \log \binom{n_B}{m_1} &= n_B \log n_B - n_B \pi_1 \log(n_B \pi_1) \\ &\quad - n_B \pi_2 \log(n_B \pi_2) + o(n_B). \end{aligned} \quad (27)$$

Since  $\pi_1 + \pi_2 = 1$ , the terms involving  $\log n_B$  cancel, and therefore

$$\begin{aligned} \log \binom{n_B}{m_1} &= -n_B \pi_1 \log \pi_1 - n_B \pi_2 \log \pi_2 + o(n_B) \\ &= n_B H(\pi_1, \pi_2) + o(n_B). \end{aligned} \quad (28)$$

To generate candidate bipartitions,  $X_B$  is projected onto the first principal-component direction and sorted by the projected values. All cut positions satisfying  $|Y_1| \geq n_{\min}$ ,  $|Y_2| \geq n_{\min}$  are regarded as feasible candidates. Let  $\mathcal{P}_2(B)$  denote the feasible candidate set along the first principal-component projection. The optimal two-ball description length is then defined as

$$L_2^*(X_B) = \min_{(Y_1, Y_2) \in \mathcal{P}_2(B)} L_2(X_B; Y_1, Y_2). \quad (29)$$

Figure 1 shows a typical situation in which a single current ball contains two local centers and is therefore better represented by two sub-balls.

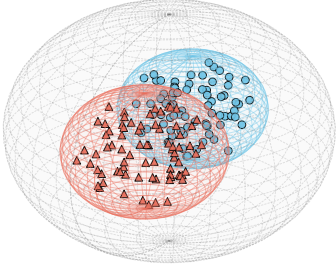


Fig. 1. Illustration of the two-ball model  $M_2$ . The current local region is better explained by two sub-balls corresponding to two local centers.

#### H. Core-Ball-Plus-Residual Model

Another type of local mismatch arises when the main body of the current ball remains single-centered, but a few peripheral samples substantially inflate the single-ball coding cost. In this case, forcing a two-ball split may break the main structure unnecessarily. To address this situation, a core-ball-plus-residual model is introduced.

The samples in  $X_B$  are sorted in ascending order of their distances to the ball center  $c_B$ :  $\|x_{(1)} - c_B\|_2 \leq \dots \leq \|x_{(n_B)} - c_B\|_2$ . For any residual size  $q \in \{1, \dots, n_B - n_{\min}\}$ , define the core set and residual set as

$$C_q = \{x_{(1)}, \dots, x_{(n_B - q)}\}, R_q = \{x_{(n_B - q + 1)}, \dots, x_{(n_B)}\}. \quad (30)$$

Let  $r_{C_q}$  denote the radius of the core set and  $r_B$  denote the radius of the current ball. The outer background radius is defined as

$$r_{\text{out}} = 2r_B. \quad (31)$$

Equation (31) sets the outer radius to twice the current-ball radius in order to preserve a shell region whose scale remains comparable to that of the current ball itself. On the one hand, this outer region is wide enough to cover peripheral samples peeled from the boundary and thus provides a reasonable background space for residual coding. On the other hand, it avoids an excessively large background expansion that would make the residual encoding artificially too permissive. Therefore, it can be viewed as a natural compromise between locality and background redundancy.

The volume of a  $d$ -dimensional Euclidean ball is

$$V_d(r) = \frac{\pi^{d/2}}{\Gamma(d/2 + 1)} r^d. \quad (32)$$

Hence, the shell volume is

$$V_{\text{shell}}(q) = V_d(r_{\text{out}}) - V_d(r_{C_q}). \quad (33)$$

Assuming that the residual points are approximately independently distributed in this shell region, the corresponding coding cost is written as

$$L_{\text{res}}(R_q | C_q) = q \log V_{\text{shell}}(q). \quad (34)$$

*Proposition 1:* If each residual point is approximately independently and uniformly distributed in the shell region, then its negative log-likelihood is equivalent to  $q \log V_{\text{shell}}(q)$ , up to an additive constant independent of the samples.

*Proof 3:* Let the shell-region volume be  $V_{\text{shell}}(q)$ . Under the uniform-background assumption, the density of a single residual point is

$$p(x | C_q) = \frac{1}{V_{\text{shell}}(q)}. \quad (35)$$

If the points in  $R_q = \{x_1, \dots, x_q\}$  are conditionally independent, then

$$p(R_q | C_q) = \prod_{i=1}^q \frac{1}{V_{\text{shell}}(q)} = V_{\text{shell}}(q)^{-q}. \quad (36)$$

Therefore, the negative log-likelihood is

$$-\log p(R_q | C_q) = q \log V_{\text{shell}}(q), \quad (37)$$

which gives Eq. (34).

Since the residual set is uniquely determined by radial peeling, only the residual-size index needs to be encoded, and its cost is defined as

$$L_{\text{idx}}(q) = \log(\max(n_B, 2)). \quad (38)$$

Accordingly, the description length of the core-ball-plus-residual model is defined as

$$L_3(X_B; q) = L_1(C_q) + q \log V_{\text{shell}}(q) + \log(\max(n_B, 2)). \quad (39)$$

All feasible residual sizes are evaluated. Let

$$\mathcal{Q}_B = \{1, \dots, n_B - n_{\min}\}, \quad (40)$$

and define the optimal core-ball-plus-residual description length as

$$L_3^*(X_B) = \min_{q \in \mathcal{Q}_B} L_3(X_B; q). \quad (41)$$

Figure 2 illustrates the basic idea of the core-ball-plus-residual model. In this case, the main body of the current local region remains single-centered and can be represented by a compact core ball, while several peripheral samples are more suitably treated as residuals.

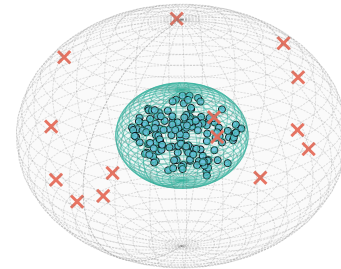


Fig. 2. Illustration of the core-ball-plus-residual model  $M_3$ . A compact core ball represents the main local structure, while peripheral samples are treated as residuals.

#### I. Criterion for Abnormal Granular Balls

Based on the above three local models, whether a current ball is abnormal can be uniformly defined as

$$M^*(B) = \arg \min\{L_1(X_B), L_2^*(X_B), L_3^*(X_B)\}. \quad (42)$$

If  $M^*(B) = M_1$ , the current ball is retained; otherwise, it is regarded as an abnormal ball and is locally regenerated according to the best competing model. Equivalently,

$$B \text{ is abnormal} \iff \min\{L_2^*(X_B), L_3^*(X_B)\} < L_1(X_B). \quad (43)$$

### J. Local Regeneration and Residual Reassignment

If  $M^*(B) = M_2$ , the current ball is regenerated into two sub-balls and both are pushed back into the processing queue. If  $M^*(B) = M_3$ , the core ball is returned to the queue while the residual subset is stored in a residual pool. If  $M^*(B) = M_1$ , the current ball is directly added to the stable set.

After all stable balls have been obtained, the residual points are globally reassigned. For any residual point  $x$  and stable ball  $B_j$ , the attachment cost is defined as

$$\Delta_j(x) = L_1(X_{B_j} \cup \{x\}) - L_1(X_{B_j}), \quad (44)$$

whereas the cost of keeping the residual point as background is

$$\Delta_{\text{bg}}(x) = \log V_{\text{bg}}, \quad (45)$$

where  $V_{\text{bg}}$  denotes the volume of the global bounding box after normalization. Each residual point is assigned to the destination with the minimum coding cost.

### K. Overall Procedure

The complete workflow of the proposed MDL-GBG framework is illustrated in Fig. 3 and summarized in Algorithm 1. Starting from the normalized dataset, a coarse-grained initial granular-ball set is first generated by recursive approximate farthest-point bisection. Each current granular ball is then evaluated under the single-ball, two-ball, and core-ball-plus-residual models. If the single-ball model remains optimal, the ball is added to the stable set. Otherwise, the ball is locally regenerated according to the best competing model and returned to the processing queue. After all stable granular balls have been obtained, the residual pool is globally reassigned by comparing attachment costs and background costs.

Algorithm 1 shows that ball generation, abnormality identification, local regeneration, and residual reassignment are all governed by the same MDL criterion. As a result, the final granular-ball structure is not determined by a handcrafted quality score, but by repeated local competition among alternative structural explanations. With this methodological framework in place, the next section evaluates whether the resulting stable granular-balls can provide an effective upstream representation for downstream clustering on benchmark datasets.

## III. COMPUTATIONAL COMPLEXITY ANALYSIS

In this section, the computational complexity of MDL-GBG is analyzed. Let  $n$  denote the number of samples and  $d$  the feature dimension. For a current granular ball  $B$ , let  $n_B$  be the number of covered samples.

---

### Algorithm 1: MDL-GBG

---

**Input:** Normalized dataset  $X \subseteq [0, 1]^d$   
**Output:** Final stable granular-ball set  $\mathcal{G}^*$  and reassigned residual set  $\mathcal{R}^*$

- 1 **Initialization:**
- 2 Generate the coarse-grained initial granular-ball set  $\mathcal{G}^{(0)}$  by recursive approximate farthest-point bisection until the number of initial balls reaches  $k_0$  ;
- 3  $\mathcal{Q} \leftarrow \mathcal{G}^{(0)}$  ; // processing queue
- 4  $\mathcal{G}^* \leftarrow \emptyset$  ; // stable granular-ball set
- 5  $\mathcal{R} \leftarrow \emptyset$  ; // residual pool
- 6 **while**  $\mathcal{Q} \neq \emptyset$  **do**
- 7 | Extract a current granular ball  $B$  from  $\mathcal{Q}$  ;
- 8 | Compute  $L_1(X_B)$  ;
- 9 | Enumerate all feasible candidate splits in  $\mathcal{P}_2(B)$  and obtain  $L_2^*(X_B)$  ;
- 10 | Enumerate all feasible residual sizes in  $\mathcal{Q}_B$  and obtain  $L_3^*(X_B)$  ;
- 11 |  $M^*(B) \leftarrow \arg \min\{L_1(X_B), L_2^*(X_B), L_3^*(X_B)\}$  ;
- 12 | **if**  $M^*(B) = M_1$  **then**
- 13 | | Add  $B$  to  $\mathcal{G}^*$  ;
- 14 | **else**
- 15 | | **if**  $M^*(B) = M_2$  **then**
- 16 | | | Regenerate  $B$  into two sub-balls  $B_1, B_2$  ;
- 17 | | | Push  $B_1$  and  $B_2$  into  $\mathcal{Q}$  ;
- 18 | | **else**
- 19 | | | Regenerate  $B$  into one core ball  $B_c$  and one residual set  $R_B$  ;
- 20 | | | Push  $B_c$  into  $\mathcal{Q}$  ;
- 21 | | |  $\mathcal{R} \leftarrow \mathcal{R} \cup R_B$  ;
- 22 | **foreach**  $x \in \mathcal{R}$  **do**
- 23 | | Compute the attachment cost  $\Delta_j(x)$  for each stable granular ball  $B_j$  ;
- 24 | | Compute the background cost  $\Delta_{\text{bg}}(x)$  ;
- 25 | | Assign  $x$  to the destination with minimum coding cost ;
- 26 **return**  $\mathcal{G}^*, \mathcal{R}^*$

---

### A. Local Complexity

For the single-ball model, computing the sample mean and the residual sum of squares requires  $O(n_B d)$ .

For the two-ball model, computing the first principal direction requires  $O(n_B d^2)$  in the common case, while projection and sorting require  $O(n_B d + n_B \log n_B)$ . Let  $S_B$  denote the number of feasible split positions. Since prefix sufficient statistics are used after sorting, evaluating all feasible cuts costs  $O(S_B d)$ . Thus,

$$\begin{aligned} T_{M_2}(B) &= O(n_B d^2 + n_B d + n_B \log n_B + S_B d) \\ &= O(n_B d^2 + n_B d + n_B \log n_B), \end{aligned} \quad (46)$$

where  $S_B \leq n_B$ .

For the core-ball-plus-residual model, sorting samples by their distances to the current center costs  $O(n_B d + n_B \log n_B)$ . Let  $R_B$  denote the number of feasible residual sizes. Since

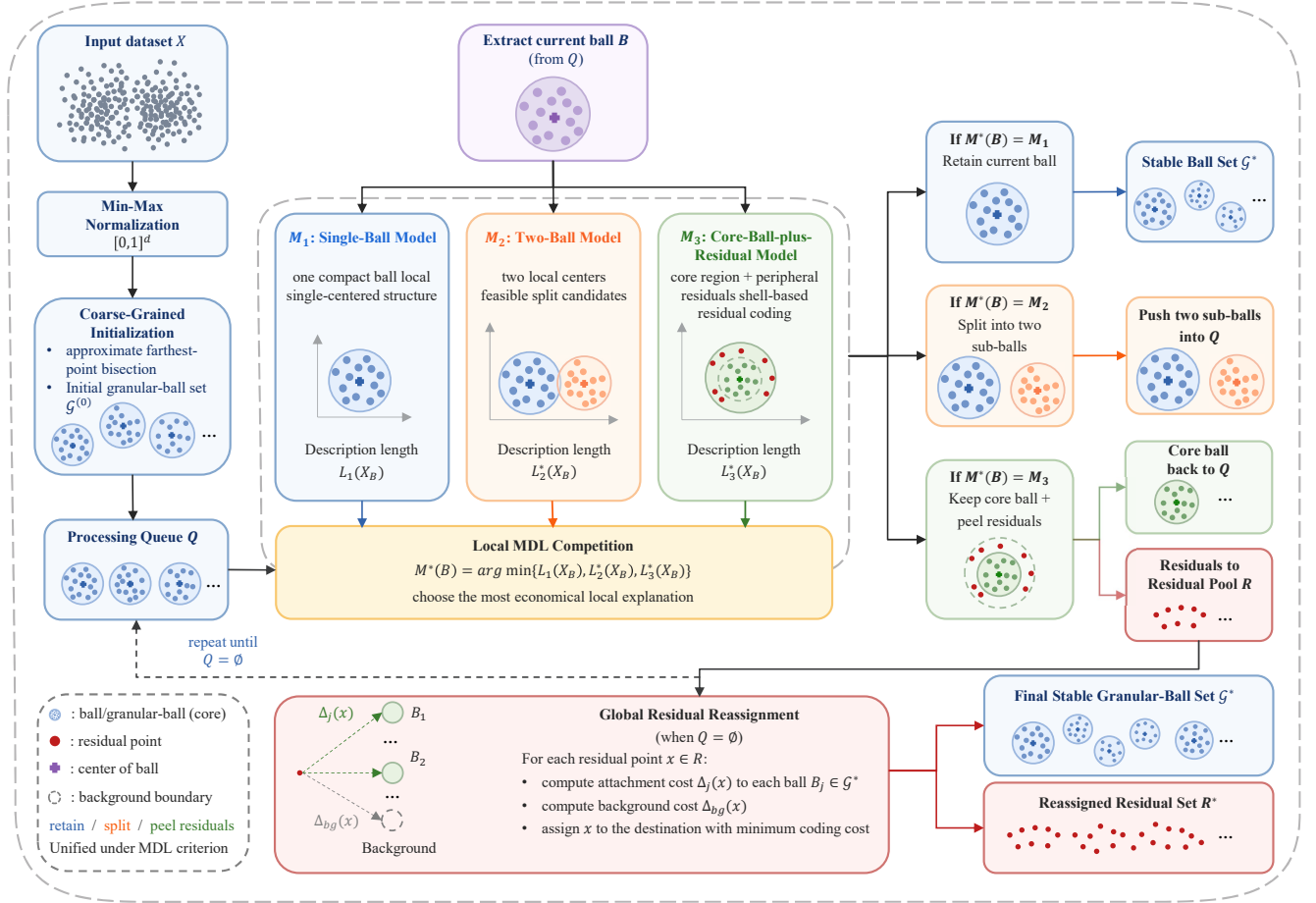


Fig. 3. Overall framework of MDL-GBG. The generation process is driven by local MDL competition among the single-ball, two-ball, and core-ball-plus-residual models, followed by residual reassignment after stable granular-balls are obtained.

the core radius is evaluated for each candidate, the candidate evaluation cost is  $O(R_B n_B d)$ . Hence,

$$\begin{aligned} T_{M_3}(B) &= O(n_B d + n_B \log n_B + R_B n_B d) \\ &= O(n_B^2 d + n_B \log n_B), \end{aligned} \quad (47)$$

where  $R_B \leq n_B$ .

Therefore, the total MDL evaluation cost for one current granular ball is

$$T_B = O(n_B d^2 + n_B^2 d + n_B \log n_B). \quad (48)$$

### B. Global Complexity

The overall procedure consists of normalization, coarse-grained initialization, recursive refinement, residual reassignment, and final sample assignment. Min-max normalization requires  $O(nd)$ . The initialization stage generates  $k_0 = \max(1, \lfloor \sqrt{n} \rfloor)$  initial balls by approximate farthest-point bisection, with a conservative upper bound  $O(n^{3/2}d)$ , which is usually dominated by the refinement stage.

Let  $n_{B_1}, n_{B_2}, \dots$  denote the sizes of all balls processed during recursive regeneration. The total refinement cost is  $\sum_B O(n_B d^2 + n_B^2 d + n_B \log n_B)$ .

Under balanced regeneration,

$$\begin{aligned} \sum_B n_B &= O(n \log n), \\ \sum_B n_B \log n_B &= O(n \log^2 n), \\ \sum_B n_B^2 &= O(n^2), \end{aligned} \quad (49)$$

which gives  $O(nd^2 \log n + n^2 d + n \log^2 n)$ .

Under highly unbalanced regeneration,

$$\begin{aligned} \sum_B n_B &= O(n^2), \\ \sum_B n_B \log n_B &= O(n^2 \log n), \\ \sum_B n_B^2 &= O(n^3), \end{aligned} \quad (50)$$

which gives  $O(n^2 d^2 + n^3 d + n^2 \log n)$ .

For residual reassignment, if  $R$  residual points and  $K$  stable granular balls are obtained, the reassignment cost is  $O(RKd)$ , bounded by  $O(n^2 d)$ . The final assignment of all samples to their nearest stable-ball centers costs  $O(nKd)$ , also bounded by  $O(n^2 d)$ .

### C. Total Time and Space Complexity

Combining the above components, the total time complexity of MDL-GBG is

$$\begin{aligned} T_{\text{balanced}} &= O(nd^2 \log n + n^2 d + n \log^2 n), \\ T_{\text{worst}} &= O(n^2 d^2 + n^3 d + n^2 \log n), \end{aligned} \quad (51)$$

where  $T_{\text{balanced}}$  and  $T_{\text{worst}}$  denote the balanced and worst-case complexities, respectively.

The space complexity is

$$S = O(nd + d^2), \quad (52)$$

where  $O(nd)$  is mainly used for data storage and local working arrays, and  $O(d^2)$  accounts for principal-direction computation.

Overall, MDL-GBG maintains polynomial complexity while avoiding full pairwise-distance storage and preserving the interpretability of local model competition.

## IV. EXPERIMENTS

### A. Experimental Settings

To evaluate the effectiveness of the proposed MDL-GBG, the stable granular-balls generated by MDL-GBG were used as the input representation for two classical clustering back-ends, namely Agglomerative Clustering (AC) and KMeans++ [23]. Let  $K$  denote the ground-truth number of clusters. If the number of stable granular-balls generated by MDL-GBG was less than or equal to  $K$ , the labels of the stable granular-balls were directly used to compute the clustering metrics. Otherwise, the stable granular-balls were further clustered into  $K$  clusters by AC or KMeans++, and the resulting labels were used for evaluation.

The comparative methods include two sample-level baselines, namely AC and KMeans++, together with four recent granular-ball clustering methods, namely GBCT [3], GBSC [8], WGBC [24], and MDMSC [25]. All experiments were conducted on 20 real UCI datasets<sup>1</sup>, whose statistics are summarized in Table I. Three widely used external evaluation metrics were adopted, namely Adjusted Rand Index (ARI) [26], clustering Accuracy (ACC), and Normalized Mutual Information (NMI) [27]. For algorithms involving randomness, 20 independent runs were conducted, and the results are reported in the form of mean  $\pm$  standard deviation. The runtime is reported as the average over 20 independent runs.

Unless otherwise specified, AC and KMeans++ were implemented using the scikit-learn library [28], whereas the other comparative granular-ball clustering methods were implemented based on the official open-source codes released by their original authors. For all comparative methods, the parameter settings recommended in the corresponding original papers were adopted, using their default parameter combinations whenever available, so as to ensure a fair comparison. The class labels were used solely for the calculation of ARI, ACC, and NMI, and were not used in any stage of clustering. As for the proposed MDL-GBG, it is a non-parametric granular-ball generation method and thus does not involve manual parameter tuning in the generation process. The cluster number  $K$  is

introduced only in the downstream clustering stage, or for direct metric computation when the number of stable granular-balls does not exceed the true number of clusters, and does not participate in the generation of stable granular-balls.

All experiments were conducted in Python 3.12 on a system equipped with an AMD Ryzen 9 8940HX CPU, an NVIDIA GeForce RTX 5070Ti GPU with 12 GB VRAM, 32 GB RAM, and a 1 TB SSD, under the Windows 11 operating system.

### B. Overall Clustering Performance

Table II summarizes the average ranks of all compared methods over the 20 UCI datasets, and Table III reports the dataset-level results in terms of ARI, ACC, and NMI. Overall, the two MDL-GBG-based pipelines achieve favorable clustering performance across the benchmark datasets. In particular, MDL-GBG+AC obtains the best average ranks on all three evaluation metrics, with ranks of 2.70, 2.90, and 2.50 on ARI, ACC, and NMI, respectively. MDL-GBG+KM++ also achieves competitive ranks of 2.95, 3.15, and 3.00. These results suggest that the stable granular-balls generated by MDL-GBG provide an effective intermediate representation for downstream clustering.

The average metric values in Table III show a similar pattern. MDL-GBG+AC achieves the highest average ARI, ACC, and NMI values among all compared methods, reaching 0.5083, 0.7556, and 0.5629, respectively. MDL-GBG+KM++ also obtains strong average results, with 0.4898 on ARI, 0.7213 on ACC, and 0.5378 on NMI. Compared with the corresponding sample-level baselines, MDL-GBG+AC improves over AC by a clear margin, while MDL-GBG+KM++ generally improves over KMeans++. This indicates that MDL-GBG does not simply reduce the number of objects to be clustered, but transforms the original samples into a more compact and structurally informative representation.

The dataset-level results further illustrate the behavior of the proposed method. MDL-GBG+AC performs well on several datasets with different scales and feature dimensions, such as Wine, Glass, Heart, Waveform, HTRU2, Shuttle, CDC, and Crop. For example, on Wine, MDL-GBG+AC achieves the best ARI, ACC, and NMI simultaneously. On HTRU2 and Crop, it also obtains the best results on multiple metrics, showing that the proposed representation can remain effective on relatively large datasets. MDL-GBG+KM++ shows favorable performance on datasets such as Segment, Rice, and PenDigits, suggesting that the generated stable granular-balls can also benefit centroid-based clustering when the obtained representation is compatible with the cluster geometry.

Compared with existing granular-ball clustering methods, MDL-GBG also shows competitive overall performance. It generally outperforms GBCT and GBSC in terms of average metric values, and remains comparable to or better than WGBC and MDMSC on many datasets. This comparison indicates that the performance gain does not come merely from using granular-balls as data units. Rather, the MDL-based local model competition helps generate stable granular-balls that are more suitable for subsequent clustering.

At the same time, the results also show that the performance of MDL-GBG depends on the structural characteristics of the

<sup>1</sup><https://archive.ics.uci.edu/>

TABLE I  
DATASET INFORMATION AND ABBREVIATIONS.

Abbr.	DataSet	Samples	Features	Classes
Zoo	Zoo	101	16	7
Iris	iris	150	4	3
Wine	Wine	178	13	3
Glass	Glass Identification	214	9	6
Heart	Statlog (Heart)	270	13	2
Ecoli	Ecoli	336	7	8
Australian	Statlog (Australian Credit Approval)	690	14	2
Segment	Statlog (Image Segmentation)	2310	19	7
Churn	Iranian Churn	3150	13	2
Rice	Rice (Cammee and Osmanicik)	3810	7	2

Abbr.	DataSet	Samples	Features	Classes
Waveform	Waveform Database Generator (Version 1)	5000	21	3
Digits	Optical Recognition of Handwritten Digits	5620	64	10
Landsat	Statlog (Landsat Satellite)	6435	36	6
Isolet	isolet	7797	617	26
PenDigits	Pen-Based Recognition of Handwritten Digits	10992	16	10
Bean	Dry Bean	13611	16	7
HTRU2	HTRU2	17898	8	2
Shuttle	Statlog (Shuttle)	58000	7	7
CDC	CDC Diabetes Health Indicators	253680	21	2
Crop	Crop mapping using fused optical-radar data set	325834	174	7

TABLE II  
AVERAGE RANKS OVER THE 20 UCI DATASETS. FOR ARI, ACC, AND NMI, A SMALLER RANK INDICATES BETTER PERFORMANCE; FOR RUNTIME, A SMALLER RANK INDICATES HIGHER EFFICIENCY.

Method	ARI	ACC	NMI	Runtime
MDL-GBG+AC	<b>2.70</b>	<b>2.90</b>	<b>2.50</b>	3.45
MDL-GBG+KM++	2.95	3.15	3.00	4.55
AC	6.10	5.95	6.00	2.40
KM++	4.60	4.60	5.00	<b>2.30</b>
WGBC	3.85	3.88	4.15	4.80
MDMSC	4.55	4.58	4.05	6.85
GBSC	5.00	5.08	5.20	4.60
GBCT	6.25	5.88	6.10	7.05

Note: ME entries are assigned the worst tied rank on the corresponding dataset.

dataset and the downstream clustering back-end. The advantage of MDL-GBG is more stable when it is combined with AC than when it is combined with KMeans++, suggesting that the local structure preserved by MDL-GBG is more naturally exploited by a hierarchical clustering procedure. In addition, on datasets with weak clusterability, class imbalance, or ambiguous global structure, the improvement may become less consistent. For instance, on Iranian Churn and CDC Diabetes Health Indicators, ACC may remain relatively high while ARI and NMI are much lower. This indicates that a high matching accuracy does not necessarily imply that the intrinsic clustering structure has been well recovered. Therefore, although MDL-GBG provides a useful upstream representation in many cases, it does not remove the intrinsic difficulty of structurally challenging datasets.

### C. Runtime Analysis

Runtime is analyzed separately because MDL-GBG is designed as a non-parametric and interpretable granular-ball generation method rather than a purely efficiency-oriented clustering algorithm. Fig. 4 and Table IV summarize the grouped average runtime over three sample-scale regimes: datasets with at most 5000 samples, datasets with more than 5000 but no more than 50000 samples, and datasets with more than 50000 samples. Fig. 5 further illustrates the relationship among sample size, feature dimensionality, and runtime for MDL-GBG+AC. Since MDL-GBG+AC and MDL-GBG+KM++ exhibit similar runtime trends, only MDL-

GBG+AC is shown in the bubble plot to avoid redundant visualization.

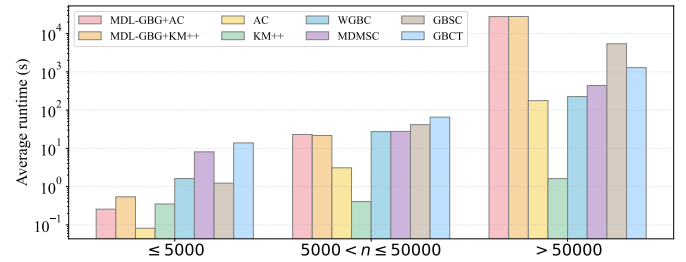


Fig. 4. Average runtime across three sample-scale regimes.

As shown in Table IV, the runtime of MDL-GBG increases with the sample scale. For MDL-GBG+AC, the grouped average runtime is 0.2574 s on datasets with no more than 5000 samples, 23.0661 s on datasets with 5000–50000 samples, and 27834.4844 s on datasets with more than 50000 samples. MDL-GBG+KM++ follows a similar trend, with grouped average runtimes of 0.5401 s, 21.6747 s, and 27972.6602 s in the three regimes. This indicates that the computational cost of MDL-based granular-ball generation grows substantially as the sample size increases.

Fig. 5 provides a more detailed view of how sample size and feature dimensionality jointly affect runtime. In this figure, the horizontal axis corresponds to the number of samples, the vertical axis corresponds to the number of features, and the runtime is encoded by both bubble color and bubble size. The distribution of bubbles shows that sample size is a major factor affecting runtime. Datasets with larger sample sizes, such as Shuttle, CDC, and Crop, require more time than most small- and medium-scale datasets. Feature dimensionality also contributes to the computational burden. For example, Isolet contains only 7797 samples but has 617 features, resulting in a much longer runtime than other datasets with a similar sample scale. Crop is the most demanding case because it combines a very large sample size with relatively high dimensionality.

From a comparative perspective, sample-level clustering methods are faster in most cases. AC is the fastest method on the small-scale group, with an average runtime of 0.0817 s. KMeans++ is the fastest method on the medium- and large-scale groups, with average runtimes of 0.4065 s and 1.6171 s, respectively. This is expected because these methods directly operate on the original samples and do not include granular-ball generation or local model selection. However, their

TABLE III  
DATASET-LEVEL COMPARISON OF ARI, ACC, AND NMI ON THE 20 UCI DATASETS.

DataSet	Metric	Ours		Baseline		Granular-Ball Methods			
		MDL-GBG +AC	MDL-GBG +KM++	AC	KM++	WGBC (ICDE 2024)	MDMSC (AAAI 2025)	GBSC (TKDE 2023)	GBCT (TNNLS 2025)
Zoo	ARI	0.8277	0.8151 ± 0.0563	0.6159	0.6625 ± 0.0913	<b>0.9403</b> ± <b>0.0228</b>	0.5442	0.1927 ± 0.1441	0.5333
	ACC	0.8614	0.8530 ± 0.0376	0.7525	0.7560 ± 0.0614	<b>0.9069</b> ± <b>0.0188</b>	0.6634	0.4346 ± 0.0724	0.6238
	NMI	0.8789	0.8738 ± 0.0227	0.7403	0.7591 ± 0.0385	<b>0.9026</b> ± <b>0.0124</b>	0.7515	0.4255 ± 0.1068	0.6026
Iris	ARI	0.6956	0.6809 ± 0.0366	0.7592	0.7219 ± 0.0070	0.7727 ± 0.0227	<b>0.9038</b>	0.6537 ± 0.0000	0.5681
	ACC	0.8733	0.8646 ± 0.0224	0.9067	0.8893 ± 0.0033	0.9133 ± 0.0106	<b>0.9667</b>	0.8467 ± 0.0000	0.6667
	NMI	0.7709	0.7516 ± 0.0430	0.8057	0.7484 ± 0.0082	0.7852 ± 0.0090	<b>0.8851</b>	0.7490 ± 0.0000	0.7337
Wine	ARI	<b>0.9472</b>	0.8431 ± 0.1430	0.2926	0.3628 ± 0.0153	0.8732 ± 0.0147	0.7414	0.5522 ± 0.0000	0.7033
	ACC	<b>0.9831</b>	0.9385 ± 0.0833	0.6124	0.6643 ± 0.0595	0.9567 ± 0.0055	0.9101	0.8146 ± 0.0000	0.8933
	NMI	<b>0.9275</b>	0.8372 ± 0.1174	0.4049	0.4257 ± 0.0063	0.8569 ± 0.0114	0.7528	0.6430 ± 0.0000	0.7397
Glass	ARI	<b>0.2937</b>	0.2210 ± 0.0314	0.0198	0.2584 ± 0.0157	0.2084 ± 0.0213	0.1651	0.1426 ± 0.0003	0.0396
	ACC	0.5234	0.4836 ± 0.0221	0.3785	<b>0.5346</b> ± <b>0.0194</b>	0.4771 ± 0.0171	0.4112	0.4206 ± 0.0000	0.4065
	NMI	<b>0.4638</b>	0.3888 ± 0.0408	0.1145	0.4030 ± 0.0224	0.3664 ± 0.0246	0.3595	0.2822 ± 0.0014	0.1608
Heart	ARI	<b>0.3757</b>	0.3107 ± 0.0734	-0.0010	0.0283 ± 0.0012	0.1668 ± 0.0123	0.1025	0.0284 ± 0.0000	0.0241
	ACC	<b>0.8074</b>	0.7759 ± 0.0485	0.5519	0.5898 ± 0.0016	0.7063 ± 0.0069	0.6630	0.5926 ± 0.0000	0.5926
	NMI	<b>0.2917</b>	0.2435 ± 0.0565	0.0002	0.0188 ± 0.0007	0.1294 ± 0.0144	0.1032	0.0723 ± 0.0000	0.0395
Ecoli	ARI	0.6866	0.5052 ± 0.0728	<b>0.7449</b>	0.4289 ± 0.0492	0.6991 ± 0.0542	0.4930	0.3211 ± 0.0374	0.5205
	ACC	<b>0.7917</b>	0.6374 ± 0.0630	0.7649	0.5632 ± 0.0439	0.7641 ± 0.0449	0.6339	0.5036 ± 0.0203	0.6607
	NMI	0.6773	0.6126 ± 0.0203	<b>0.7193</b>	0.6034 ± 0.0264	0.6580 ± 0.0293	0.6218	0.4765 ± 0.0353	0.5696
Australian	ARI	0.4277	0.3414 ± 0.1031	0.0007	0.0031 ± 0.0008	<b>0.4802</b> ± <b>0.0353</b>	0.0215	0.0859 ± 0.0815	-0.0030
	ACC	0.8275	0.7882 ± 0.0517	0.5565	0.5610 ± 0.0015	<b>0.8465</b> ± <b>0.0135</b>	0.5826	0.6338 ± 0.0708	0.5348
	NMI	0.3533	0.2754 ± 0.0909	0.0034	0.0134 ± 0.0032	<b>0.4049</b> ± <b>0.0337</b>	0.0133	0.1115 ± 0.0813	0.0676
Segment	ARI	0.4735	<b>0.4888</b> ± <b>0.0424</b>	0.0001	0.3381 ± 0.0576	0.0000 ± 0.0000	0.0811	0.4754 ± 0.0142	0.3747
	ACC	0.5814	<b>0.6261</b> ± <b>0.0532</b>	0.1459	0.5027 ± 0.0589	0.1429 ± 0.0000	0.2584	0.6119 ± 0.0187	0.5346
	NMI	<b>0.6776</b>	0.6190 ± 0.0262	0.0153	0.5094 ± 0.0478	0.0000 ± 0.0000	0.3338	0.6379 ± 0.0199	0.5732
Churn	ARI	-0.0209	0.3663 ± 0.0263	-0.0834	-0.1074 ± 0.0000	<b>0.3941</b> ± <b>0.0348</b>	0.0086	0.3577 ± 0.0000	0.3377
	ACC	0.8289	0.8364 ± 0.0213	0.7622	0.6680 ± 0.0007	0.8645 ± 0.0327	0.4987	0.8295 ± 0.0000	<b>0.8832</b>
	NMI	0.0095	0.2260 ± 0.0286	0.0403	0.0738 ± 0.0003	<b>0.2482</b> ± <b>0.0304</b>	0.0064	0.2167 ± 0.0000	0.2322
Rice	ARI	0.5808	<b>0.6881</b> ± <b>0.0020</b>	0.5413	0.5776 ± 0.0004	0.6755 ± 0.0000	0.6753	0.6824 ± 0.0000	-0.0021
	ACC	0.8814	<b>0.9148</b> ± <b>0.0006</b>	0.8682	0.8802 ± 0.0001	0.9110 ± 0.0000	0.9110	0.9131 ± 0.0000	0.5677
	NMI	0.5002	<b>0.5748</b> ± <b>0.0023</b>	0.4633	0.4690 ± 0.0004	0.5632 ± 0.0000	0.5709	0.5694 ± 0.0000	0.0052
Waveform	ARI	<b>0.4209</b>	0.3566 ± 0.0921	0.2980	0.2651 ± 0.0513	0.3770 ± 0.0932	0.2512	0.2518 ± 0.0000	0.1181
	ACC	<b>0.7418</b>	0.6496 ± 0.1001	0.5574	0.5154 ± 0.0613	0.6687 ± 0.1252	0.5224	0.5150 ± 0.0000	0.5110
	NMI	<b>0.4529</b>	0.4211 ± 0.0449	0.3878	0.3687 ± 0.0292	0.4193 ± 0.0419	0.3592	0.3702 ± 0.0000	0.2312
Digits	ARI	0.6326	0.6511 ± 0.0502	0.5703	0.6297 ± 0.0442	0.3191 ± 0.0170	<b>0.8333</b>	0.2876 ± 0.0017	0.0003
	ACC	0.7418	0.7600 ± 0.0566	0.6349	0.7493 ± 0.0476	0.4979 ± 0.0267	<b>0.8776</b>	0.4376 ± 0.0030	0.1181
	NMI	0.7738	0.7438 ± 0.0277	0.7617	0.7332 ± 0.0211	0.4824 ± 0.0154	<b>0.9029</b>	0.4597 ± 0.0044	0.0426
Landsat	ARI	0.3583	0.5264 ± 0.0111	0.2734	0.4883 ± 0.0739	<b>0.5608</b> ± <b>0.0171</b>	0.5599	0.4819 ± 0.0027	0.0005
	ACC	0.6117	0.6732 ± 0.0104	0.4923	0.6505 ± 0.0604	<b>0.7247</b> ± <b>0.0176</b>	0.7120	0.7157 ± 0.0013	0.2415
	NMI	0.5115	0.6090 ± 0.0028	0.4264	0.5837 ± 0.0501	0.6100 ± 0.0103	<b>0.6567</b>	0.5748 ± 0.0027	0.0100
Isolet	ARI	0.4471	0.4585 ± 0.0236	0.1460	<b>0.4751</b> ± <b>0.0268</b>	0.1922 ± 0.0069	0.4599	0.1560 ± 0.0132	0.0078
	ACC	0.5153	0.5303 ± 0.0237	0.2138	0.5425 ± 0.0273	0.3065 ± 0.0076	<b>0.5639</b>	0.2454 ± 0.0072	0.1075
	NMI	0.7315	0.7194 ± 0.0135	0.5799	0.7224 ± 0.0093	0.4671 ± 0.0086	<b>0.7600</b>	0.4236 ± 0.0113	0.2159
PenDigits	ARI	0.4410	<b>0.5720</b> ± <b>0.0320</b>	0.4139	0.5609 ± 0.0281	0.0000 ± 0.0000	0.4107	0.4247 ± 0.0002	0.0014
	ACC	0.5977	<b>0.7166</b> ± <b>0.0368</b>	0.5548	0.7063 ± 0.0455	0.1041 ± 0.0000	0.5759	0.5741 ± 0.0001	0.1398
	NMI	0.6617	0.6995 ± 0.0144	0.6517	0.6827 ± 0.0084	0.0000 ± 0.0000	<b>0.7001</b>	0.5970 ± 0.0004	0.0775
Bean	ARI	0.5324	0.6079 ± 0.0256	0.2487	0.3800 ± 0.0122	0.0000 ± 0.0000	0.6303	<b>0.6679</b> ± <b>0.0000</b>	0.0978
	ACC	0.6545	0.7355 ± 0.0362	0.3978	0.5572 ± 0.0151	0.2605 ± 0.0000	0.7598	<b>0.7969</b> ± <b>0.0000</b>	0.3377
	NMI	0.6983	0.6965 ± 0.0097	0.4511	0.5150 ± 0.0031	0.0000 ± 0.0000	<b>0.7329</b>	0.7274 ± 0.0000	0.1868
HTRU2	ARI	<b>0.6201</b>	0.5233 ± 0.0000	-0.0006	-0.0780 ± 0.0002	0.3376 ± 0.0004	0.5272	0.6049 ± 0.0002	0.0324
	ACC	<b>0.9549</b>	0.9171 ± 0.0000	0.9076	0.7659 ± 0.0011	0.9044 ± 0.0001	0.9161	0.9383 ± 0.0000	0.9103
	NMI	<b>0.4943</b>	0.3299 ± 0.0000	0.0000	0.0267 ± 0.0002	0.1528 ± 0.0003	0.3406	0.3971 ± 0.0002	0.0277
Shuttle	ARI	<b>0.5695</b>	0.1843 ± 0.0406	0.0007	0.3802 ± 0.1351	0.0000 ± 0.0000	-0.0098	0.1852 ± 0.0000	0.4534
	ACC	0.7603	0.4246 ± 0.0655	0.7859	<b>0.8047</b> ± <b>0.0279</b>	0.7860 ± 0.0000	0.3077	0.7330 ± 0.0000	0.7662
	NMI	<b>0.5800</b>	0.3878 ± 0.0244	0.0007	0.2084 ± 0.0754	0.0000 ± 0.0000	0.0086	0.3749 ± 0.0000	0.4784
CDC	ARI	<b>0.1550</b>	0.0825 ± 0.0169	ME	0.1138 ± 0.0064	0.0846 ± 0.0139	ME	ME	0.0032
	ACC	0.8024	0.6515 ± 0.0231	ME	0.7971 ± 0.0086	0.6675 ± 0.0324	ME	ME	<b>0.8548</b>
	NMI	0.0443	<b>0.0762</b> ± <b>0.0149</b>	ME	0.0255 ± 0.0022	0.0701 ± 0.0161	ME	ME	0.0002
Crop	ARI	<b>0.7017</b>	0.5737 ± 0.0228	ME	0.1298 ± 0.0186	0.0000 ± 0.0000	ME	ME	0.0657
	ACC	<b>0.7718</b>	0.6486 ± 0.0193	ME	0.3482 ± 0.0129	0.2611 ± 0.0000	ME	ME	0.3209
	NMI	<b>0.7581</b>	0.6704 ± 0.0085	ME	0.2258 ± 0.0258	0.0000 ± 0.0000	ME	ME	0.1373
Average	ARI	<b>0.5083</b>	0.4898 ± 0.0451	0.2689	0.3310 ± 0.0318	0.3541 ± 0.0183	0.4111	0.3640 ± 0.0164	0.1938
	ACC	<b>0.7556</b>	0.7213 ± 0.0388	0.6025	0.6523 ± 0.0279	0.6335 ± 0.0180	0.6519	0.6421 ± 0.0108	0.5336
	NMI	<b>0.5629</b>	0.5378 ± 0.0305	0.3648	0.4058 ± 0.0190	0.3558 ± 0.0129	0.4922	0.4505 ± 0.0146	0.2566

ME denotes MemoryError. Average values are computed over the datasets with valid numerical results.

TABLE IV  
GROUPED AVERAGE RUNTIME (SECONDS) ACROSS DIFFERENT SAMPLE-SCALE REGIMES.

Sample scale	MDL-GBG+AC	MDL-GBG+KM++	AC	KM++	WGBC	MDMSC	GBSC	GBCT
$\leq 5000$	0.2574	0.5401	<b>0.0817</b>	0.3515	1.6277	8.0995	1.2328	13.8824
$5000 < n \leq 50000$	23.0661	21.6747	3.1032	<b>0.4065</b>	27.4582	27.7924	41.5725	65.2882
$> 50000$	27834.4844	27972.6602	176.6339 <sup>a</sup>	<b>1.6171</b>	225.8146	438.9400 <sup>a</sup>	5427.3152 <sup>a</sup>	1287.4568

<sup>a</sup> The average is computed over executable datasets only. For AC, MDMSC, and GBSC, the results on CDC and Crop are unavailable due to MemoryError.

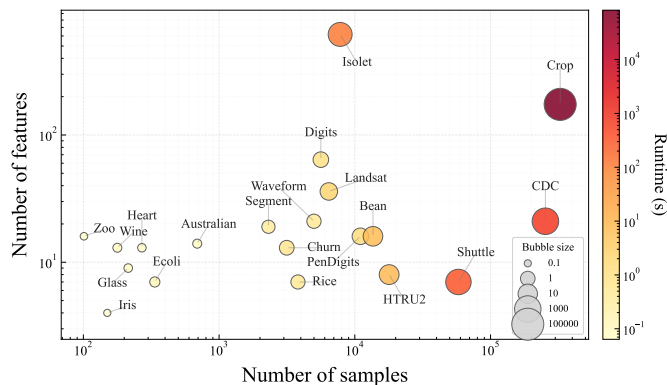


Fig. 5. Effect of sample size and feature dimensionality on the runtime of MDL-GBG+AC.

runtime advantage is accompanied by weaker average clustering performance, as reflected by their lower average ranks and average metric values in Tables II and III.

Among granular-ball clustering methods, MDL-GBG is not the most efficient method, especially on large-scale datasets. Its runtime is higher than that of WGBC, MDMSC, and GBCT in the large-scale group. This is related to the additional cost introduced by local MDL-based model competition. However, the comparison should also consider memory robustness. AC, MDMSC, and GBSC fail on CDC and Crop due to MemoryError, and their large-scale averages are computed only over executable datasets. In contrast, MDL-GBG produces results on all 20 datasets. Therefore, the large-scale runtime comparison reflects not only computational speed, but also whether a method can complete the clustering process under the given memory constraints.

The runtime behavior is consistent with the design objective of MDL-GBG. The method evaluates alternative local explanations, including the single-ball, two-ball, and core-ball-plus-residual models, to determine the local granular structure. This process increases computational cost, but it also provides a more principled and interpretable mechanism for generating stable granular-balls. The clustering results show that this additional computation can lead to better downstream clustering quality. Thus, MDL-GBG should be understood as a representation-quality-oriented method rather than a speed-oriented method.

Overall, the runtime results show that sample size is the primary factor driving computational growth, while feature dimensionality can further amplify the runtime on high-dimensional datasets. This observation also points to a practical direction for future work: improving the efficiency of local MDL evaluation, candidate structure search, and high-

dimensional distance computation, especially for large-scale or high-dimensional datasets.

## V. DISCUSSION AND CONCLUSIONS

The experimental results suggest that the effectiveness of granular-ball clustering depends not only on whether granular-balls are used, but also on how they are generated. From this perspective, the main contribution of MDL-GBG is not simply to provide another granular-ball construction strategy, but to formulate granular-ball generation as a local model selection problem under the Minimum Description Length principle. Under this formulation, retaining a ball, splitting a ball, and peeling residual samples are no longer treated as separate operations governed by independent empirical rules. Instead, these decisions are compared within a unified coding-theoretic framework.

This reformulation improves the interpretability of the generation process. In many existing granular-ball methods, the final balls may be geometrically meaningful, but the reasons why a local region is retained, divided, or refined are often implicit. By contrast, MDL-GBG explains each local regeneration decision through competition among three candidate local explanations: the single-ball model, the two-ball model, and the core-ball-plus-residual model. Therefore, the interpretability of MDL-GBG lies not only in the final granular-ball representation, but also in the decision mechanism by which the representation is produced.

The experimental results further show that this formulation is practically useful for clustering. MDL-GBG+AC obtains the best average ranks on ARI, ACC, and NMI among all compared methods, and MDL-GBG+KM++ also achieves competitive average ranks. These results indicate that the stable granular-balls generated by MDL-GBG can provide an effective upstream representation for downstream clustering. The difference between MDL-GBG+AC and MDL-GBG+KM++ is also informative. Although both pipelines benefit from the proposed generation mechanism, the performance of MDL-GBG+AC is more stable, suggesting that the local structures preserved by MDL-GBG are more naturally exploited by hierarchical aggregation than by centroid-based partitioning.

At the same time, the proposed method should not be interpreted as universally superior across all datasets and all clustering scenarios. Its advantage becomes less consistent on datasets with weak intrinsic cluster structure, strong imbalance, or ambiguous global distributions. In such cases, a high ACC value may coexist with relatively low ARI or NMI, indicating that the matched labels do not necessarily reflect a well-recovered intrinsic partition. Therefore, MDL-GBG does not

remove the inherent difficulty of challenging clustering tasks. Rather, it provides a more principled and interpretable upstream representation that can improve clustering quality when the generated local structures are compatible with the underlying data organization.

The runtime results also clarify the methodological position of MDL-GBG. Compared with sample-level KMeans++ and AC, MDL-GBG introduces additional computation because it evaluates multiple local structural hypotheses during granular-ball generation. This makes MDL-GBG less suitable as a purely speed-oriented method. The grouped runtime results show that sample size is the main factor driving computational growth, while high feature dimensionality can further increase the cost, as illustrated by the runtime behavior on high-dimensional datasets such as Isolet and large-scale datasets such as CDC and Crop. This efficiency-performance trade-off is consistent with the design goal of MDL-GBG: the method emphasizes representation quality, non-parametric generation, and interpretability rather than minimizing raw runtime.

Several limitations should be noted. First, the single-ball model is based on an isotropic Gaussian assumption, which may not fully characterize anisotropic, manifold-like, or strongly curved local structures. Second, the current candidate split mechanism is still relatively simple, relying mainly on principal-direction projection and feasible cut enumeration. Although this design keeps the method interpretable and implementable, richer structural hypotheses may be needed for more complex data distributions. Third, while MDL-GBG itself does not require manually tuned generation thresholds, the overall clustering pipeline still uses the ground-truth number of clusters in the downstream clustering stage for evaluation. Developing a fully end-to-end non-parametric clustering framework remains an important open direction.

Overall, this study shows that granular-ball generation can be treated as a principled model selection problem rather than a purely heuristic preprocessing step. By comparing explicit local structural hypotheses under a unified MDL criterion, MDL-GBG reduces the dependence on handcrafted generation rules and makes local regeneration decisions more interpretable. Experiments on 20 UCI datasets demonstrate that the stable granular-balls generated by MDL-GBG provide a useful upstream representation for clustering, especially when combined with AC. The results also indicate that the benefits of MDL-based local model competition should be understood together with its computational cost, particularly on large-scale and high-dimensional datasets.

Future work will focus on three aspects. The first is to introduce richer local structural hypotheses that can better describe anisotropic or nonlinear data regions while preserving the interpretability of MDL-based model selection. The second is to improve the efficiency of local MDL evaluation, candidate structure search, and high-dimensional distance computation for large-scale datasets. The third is to integrate MDL-GBG more tightly with downstream clustering so that the cluster number can be inferred within a more complete non-parametric framework rather than being supplied externally.

#### CREDIT AUTHORSHIP CONTRIBUTION STATEMENT

**Zeqiang Xian:** Conceptualization, Methodology, Writing – original draft, Software, Validation. **Caihui Liu:** Conceptualization, Methodology, Writing – review & editing, Validation, Supervision. **Yong Zhang:** Software, Data curation. **Wenjing Qiu:** Software, Data curation. **Duoqian Miao:** Writing – review & editing **Witold Pedrycz:** Writing – review & editing

#### DECLARATION OF COMPETING INTEREST

The authors declare that they have no known competing financial interests or personal relationships that could have appeared to influence the work reported in this paper.

#### DATA AVAILABILITY

Data will be made available on request.

#### ACKNOWLEDGMENT

The research is supported by the National Natural Science Foundation of China under Grant No. 62566003, Graduate Innovation Funding Program of Jiangxi Province under Grant No. YC2025-S224.

#### REFERENCES

- [1] L. Ding, C. Li, D. Jin, and S. Ding, "Survey of spectral clustering based on graph theory," *Pattern Recognition*, vol. 151, p. 110366, 2024.
- [2] L. Hu, M. Jiang, J. Dong, X. Liu, and Z. He, "Interpretable clustering: A survey," *ACM Computing Surveys*, vol. 58, no. 8, pp. 1–21, 2026.
- [3] S. Xia, B. Shi, Y. Wang, J. Xie, G. Wang, and X. Gao, "Gbc: efficient and adaptive clustering via granular-ball computing for complex data," *IEEE Transactions on Neural Networks and Learning Systems*, vol. 36, no. 7, pp. 12 159–12 172, 2025.
- [4] L. Chen, "Topological structure in visual perception," *Science*, vol. 218, no. 4573, pp. 699–700, 1982.
- [5] S. Xia, Y. Liu, X. Ding, G. Wang, H. Yu, and Y. Luo, "Granular ball computing classifiers for efficient, scalable and robust learning," *Information Sciences*, vol. 483, pp. 136–152, 2019.
- [6] S. Xia, G. Wang, X. Gao, and X. Lian, "Granular-ball computing: an efficient, robust, and interpretable adaptive multi-granularity representation and computation method," *arXiv preprint arXiv:2304.11171*, 2023.
- [7] S. Xia, X. Lian, G. Wang, X. Gao, Q. Hu, and Y. Shao, "Granular-ball fuzzy set and its implement in svm," *IEEE Transactions on Knowledge and Data Engineering*, vol. 36, no. 11, pp. 6293–6304, 2024.
- [8] J. Xie, W. Kong, S. Xia, G. Wang, and X. Gao, "An efficient spectral clustering algorithm based on granular-ball," *IEEE Transactions on Knowledge and Data Engineering*, vol. 35, no. 9, pp. 9743–9753, 2023.
- [9] D. Cheng, Y. Li, S. Xia, G. Wang, J. Huang, and S. Zhang, "A fast granular-ball-based density peaks clustering algorithm for large-scale data," *IEEE Transactions on Neural Networks and Learning Systems*, vol. 35, no. 12, pp. 17 202–17 215, 2023.
- [10] D. Cheng, C. Zhang, Y. Li, S. Xia, G. Wang, J. Huang, S. Zhang, and J. Xie, "Gb-dbscan: A fast granular-ball based dbscan clustering algorithm," *Information Sciences*, vol. 674, p. 120731, 2024.
- [11] Q. Wang and M. Du, "Structure-aware granular ball clustering," *Information Sciences*, vol. 740, p. 123224, 2026.
- [12] P. Su, S. Huang, W. Ma, D. Xiong, and J. Lv, "Multi-view granular-ball contrastive clustering," in *Proceedings of the AAAI Conference on Artificial Intelligence*, vol. 39, no. 19, 2025, pp. 20 637–20 645.
- [13] S. Xia, X. Dai, G. Wang, X. Gao, and E. Giem, "An efficient and adaptive granular-ball generation method in classification problem," *IEEE Transactions on Neural Networks and Learning Systems*, vol. 35, no. 4, pp. 5319–5331, 2022.
- [14] Q. Xie, Q. Zhang, S. Xia, F. Zhao, C. Wu, G. Wang, and W. Ding, "Gbg++: A fast and stable granular ball generation method for classification," *IEEE Transactions on Emerging Topics in Computational Intelligence*, vol. 8, no. 2, pp. 2022–2036, 2024.

- [15] W. Liao, Q. Zhang, Q. Xie, M. Gao, and P. Jin, "A new adaptive and effective granular ball generation method for classification," *International Journal of Machine Learning and Cybernetics*, vol. 16, no. 5, pp. 3501–3520, 2025.
- [16] F. Liu, Q. Zhang, S. Xia, Q. Xie, W. Liao, and S. Zhang, "A granular-ball generation method based on local density for classification," *Information Sciences*, vol. 717, p. 122295, 2025.
- [17] J. Pan, G. Lang, Q. Xiao, and T. Yang, "A framework of granular-ball generation for classification via granularity tuning," *Applied Intelligence*, vol. 55, no. 1, p. 63, 2025.
- [18] Z. Jia, Z. Zhang, and W. Pedrycz, "Generation of granular-balls for clustering based on the principle of justifiable granularity," *IEEE Transactions on Cybernetics*, vol. 55, no. 4, pp. 1687–1700, 2025.
- [19] W. Li, L. Wei, W. Pedrycz, W. Ding, C. Zhang, T. Zhan, and S. Xia, "Granular-ball regeneration clustering with principle of justifiable granularity," *IEEE Transactions on Neural Networks and Learning Systems*, vol. 36, no. 10, pp. 18 173–18 187, 2025.
- [20] R. Luo, T. Li, R. Pu, J. Yang, D. Tang, and L. Yang, "Nagb-dbscan: An improved dbscan clustering algorithm by natural neighbor and granular-ball," *Information Sciences*, vol. 719, p. 122445, 2025.
- [21] A. Barron, J. Rissanen, and B. Yu, "The minimum description length principle in coding and modeling," *IEEE transactions on information theory*, vol. 44, no. 6, pp. 2743–2760, 1998.
- [22] P. D. Grünwald, *The minimum description length principle*. MIT press, 2007.
- [23] D. Arthur, S. Vassilvitskii *et al.*, "k-means++: The advantages of careful seeding," in *Soda*, vol. 7, 2007, pp. 1027–1035.
- [24] J. Xie, C. Hua, S. Xia, Y. Cheng, G. Wang, and X. Gao, "W-gbc: An adaptive weighted clustering method based on granular-ball structure," in *2024 IEEE 40th International conference on data engineering (ICDE)*. IEEE, 2024, pp. 914–925.
- [25] Z. Xu, Z. Long, and H. Meng, "Clustering by mining density distributions and splitting manifold structure," in *Proceedings of the AAAI Conference on Artificial Intelligence*, vol. 39, no. 20, 2025, pp. 21 842–21 849.
- [26] W. M. Rand, "Objective criteria for the evaluation of clustering methods," *Journal of the American Statistical association*, vol. 66, no. 336, pp. 846–850, 1971.
- [27] A. Strehl and J. Ghosh, "Cluster ensembles—a knowledge reuse framework for combining multiple partitions," *Journal of machine learning research*, vol. 3, no. Dec, pp. 583–617, 2002.
- [28] F. Pedregosa, G. Varoquaux, A. Gramfort, V. Michel, B. Thirion, O. Grisel, M. Blondel, P. Prettenhofer, R. Weiss, V. Dubourg *et al.*, "Scikit-learn: Machine learning in python," *the Journal of machine Learning research*, vol. 12, pp. 2825–2830, 2011.